Molecular engineering of liquid crystalline derivatives of 6-oxoverdazyl

Piotr Kaszyński,[a,b,c]* Marcin Jasiński,[b] Sylwia Ciastek,[b] Szymon Kapuściński,[b] and Krzysztof Gębicki[b ‡]

[a] *Organic Materials Research Group, Centre for Molecular and Macromolecular Studies, Polish Academy of Sciences, Sienkiewicza 112, 90-363, Łódź, Poland*
[b] *Faculty of Chemistry, University of Łódź, Tamka 12, 91-403 Łódź, Poland*
[c] *Department of Chemistry, Middle Tennessee State University, Murfreesboro, TN 37123*
[‡] *Dr. Krzysztof Gębicki passed away in September 2015*
Email: *piotrk@cbmm.lodz.pl*

*Dedicated to Professor Jacek Młochowski on the occasion of his 80*[th] *anniversary*

Abstract

6-Oxoverdazyl, a π-delocalized stable radical, is considered a central structural element of paramagnetic self-organizing materials. The three available positions on the heterocycle can be substituted with wedge-shaped or rod-like groups in combination with a small substituent, which leads to different molecular architectures and diverse organization of the mesophase. Several of these architectures have been realized experimentally and materials exhibiting columnar and calamitic phases have been obtained. Compounds with some other combination of substituents did not exhibit liquid crystalline behavior. The analysis also indicates some new molecular architectures potentially suitable for the formation of liquid crystalline phases. Finally, results on magnetic susceptibility and photovoltaic measurements of the discotic derivatives are discussed.
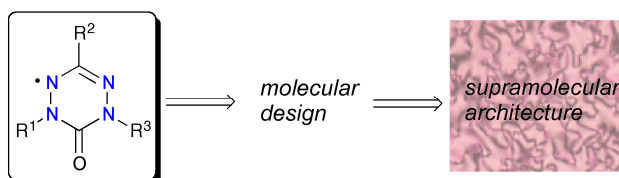
Introduction

Liquid crystals containing organic paramagnetic centers are an attractive and increasingly important class of molecular materials. The combination of magnetic behavior, favorable redox properties, and low excitation energies of π-delocalized radicals[1] with anisotropic fluid medium of the liquid crystal offers materials not only of fundamental interest, but also for potential practical applications.[2] For instance, coupling of magnetic and electronic properties with anisotropic charge transport, dielectric switching, and photo-alignment yields materials that are of particular interest for organic photovoltaics, molecular electronics, and spintronics. Recently, we initiated a research program focused on investigation of liquid crystalline radicals, and this account describes a critical analysis of the suitability of 6-oxoverdazyl (**I**) as a structural element of mesogenic compounds.
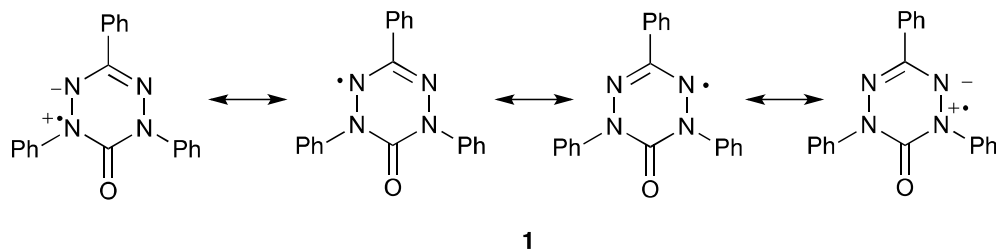
The 6-Oxoverdazyl

Verdazyls,[3] including 6-oxoverdazyls (**I**, Figure 1), are among a handful of π-delocalized radicals that are stable under ambient conditions.[1,4] They exhibit broad absorption bands in the visible part of the spectrum and an electrochemical window of about 1.45 V.[5-7] Some verdazyl derivatives have been investigated as components of paramagnetic semiconductors,[8,9] and in photo-excited molecular systems[10,11] intended for photo-magnetic devices.[12]
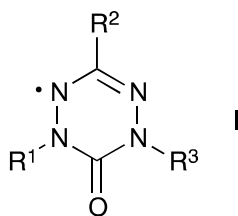

**Figure 1**. General structure of 6-oxoverdazyl (**I**).

From an applications point of view, 1,3,5-triaryl-6-oxoverdazyls are particularly attractive due to their robustness and relatively straightforward synthesis.[13,14] The prototypical 1,3,5-triphenyl-6-oxoverdazyl[15] (**1**) melts in a range 210-211 ^{o}C and is stable for hours in boiling benzene in the presence of oxygen. At higher temperatures, verdazyls, including **1**, have a tendency for slow decomposition.[16] Radical **1** has a small dipole moment (0.77 D calculated at the UB3LYP/6-31G(2d,p) level of theory), oriented along the C=O group. Analysis of the electronic structure of **1** demonstrates that the spin is localized primarily on the four nitrogen atoms, while position C(3) is a nodal point (Figure 2). Further delocalization of the spin onto the benzene rings at N(1) and N(5) positions occurs to some extent through appropriate dipolar resonance structures. This qualitative understanding of spin distribution in **1** is in agreement with DFT spin density map (Figure 3) and is well reflected in EPR spectra, which show nine principal lines broadened by additional *hfcc* to H atoms (Figure 4).

1

Figure 2. Major resonance structures for 1,3,5-triphenyl-6-oxoverdazyl (**1**).

α-HOMO, E = -5.14 eV   α-LUMO, E = -1.15 eV   spin density map
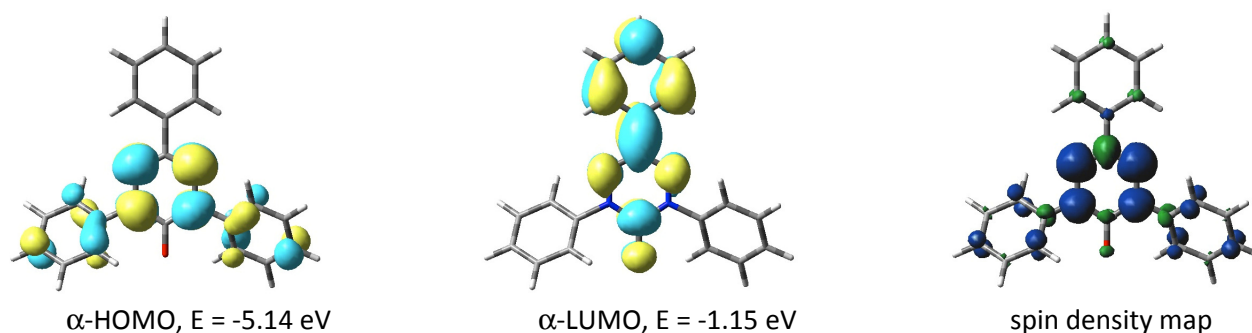
Figure 3. Contours for α-FMOs and spin density map calculated for 1,3,5-triphenyl-6-oxoverdazyl (**1**) at the UB3LYP/6-31G(2d,p) level of theory.

3310   3320   3330   3340   3350   3360   3370   3380   3390
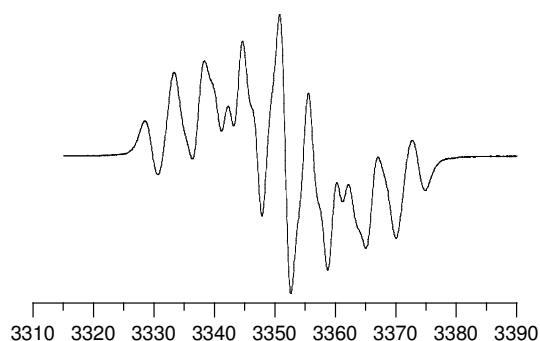
Figure 4. EPR spectrum of 1,3,5-triphenyl-6-oxoverdazyl (**1**) in CH_2Cl_2.

The geometry of the 6-oxoverdazyl ring and the conformational preferences of its substituents are important factors considered in the designing of liquid crystalline materials and for understanding their thermal behavior. Thus the experimental structure of **1**, well reproduced by DFT calculations, has the C_2 symmetry in which the phenyl substituents form interplanar angles of 38° (N(1)/N(5)-Ph) and 12° (C(3)-Ph) with the central planar verdazyl ring (Figure 5).[15]
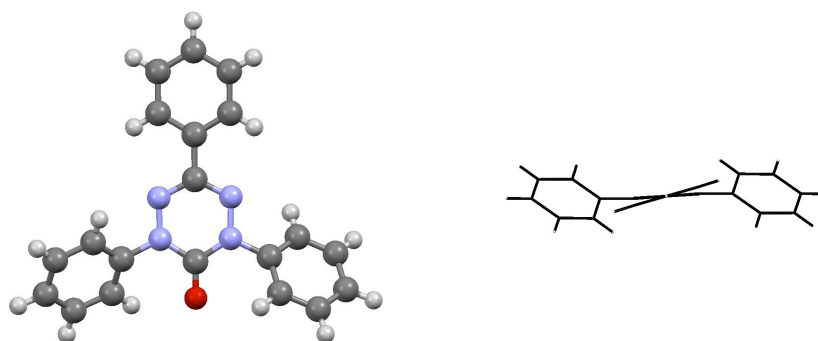
Figure 5. Two views of the experimental molecular structure of 1,3,5-triphenyl-6-oxoverdazyl (**1**) based on literature coordinates.[15]

All 6-oxoverdazyl derivatives are highly colored due to low intensity broad absorption bands in the visible range of the spectrum. The position of the bands, hence the color of the solutions, are strongly substituent-dependent.[7] TD-DFT analysis demonstrates that the lowest energy excitation is typically related to the β-HOMO to β-LUMO transition. For instance, TD-DFT calculations for **1** show that the lowest energy excitation occurs at 535 nm and involves β-FMOs (Figure 6), while the SOMO to α-LUMO excitation is calculated at 433 nm in acetonitrile dielectric medium.

β-HOMO, E = -6.16 eV   β-LUMO, E = -2.88 eV
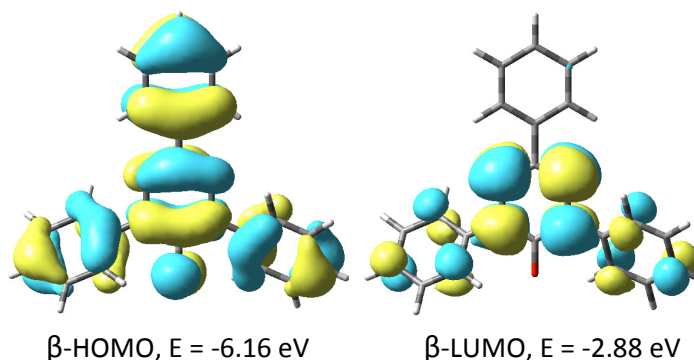
Figure 6. Contours and energies for β-FMOs involved in low energy excitations in a 1,3,5-triphenyl-6-oxoverdazyl (**1**) calculated at the UB3LYP/6-31G(2d,p) level of theory in acetonitrile dielectric medium.

The Molecular Design

Analysis of the molecular structure suggests that a 6-oxoverdazyl (**I**) can be used as a structural element for the design of liquid crystalline materials. Thus, using either wedge-shaped groups or rod-like substituents with terminal alkyl chains a number of topologies[17] can be envisioned according to general rules for mesogenic compounds.[18,19] Substitution of **I** in positions 1, 3, and 5 with wedge-shaped groups, such as 3,4,5-trialkoxy- or 3,4,5-trialkylsulfanylphenyl groups with a total of nine alkyl chains, gives rise to disk-like molecules (**A** in Chart I) that can self-assemble into columns.[20] Alternatively, substitution of the 6-oxoverdazyl (**I**) core with only two wedge-shaped groups and one small substituent R in position C(3) leads to half-disk molecular shapes (structure **B** in Chart I). Such molecules can self-assemble into columns, as it was recently demonstrated.[21] The wedge-shaped groups in **B** can be connected with the verdazyl core through a rigid bridge forming polycatenar

structures such as **C**, as demonstrated for other systems.[22,23] The mesogenicity-inducing groups in **B** and **C** can be also connected at positions 1,3 instead of in 1,5. Replacement of three wedge-shaped groups in **A** with rod-like substituents ("arms") leads to star-shaped derivatives **D** (e.g. hekates), which for other core elements typically form discotic nematic (N_D) phases.[24]

Exchanging one of the rod-like substituents in **D** for a small group R in position C(3) or N(5) leads to bent-core molecules with structure **E** or **E'**, respectively. Such molecular shapes are conducive to the formation of banana phases.[25,26] Shortening of one of the "arms" in structure **E** leads to a hockey stick molecular shape[27] (**F**), in which molecular arrangement in the mesophase is frustrated from that typical for calamitic or banana phases.

In principle, a classical rod-like molecular structure of 6-oxoverdazyls can be designed using one long substituent in position C(3) or N(1) and two small groups in the remaining two positions. The smallest of the substituents, the CH_3 group, is unsuitable due to its reactivity in the fluid phase.[28,29] Larger substituents have greater chemical stability, but cause a decrease of the molecular aspect ratio and are unfavorable for the formation of calamitic phases. For these reasons such a topology is not considered at this time.
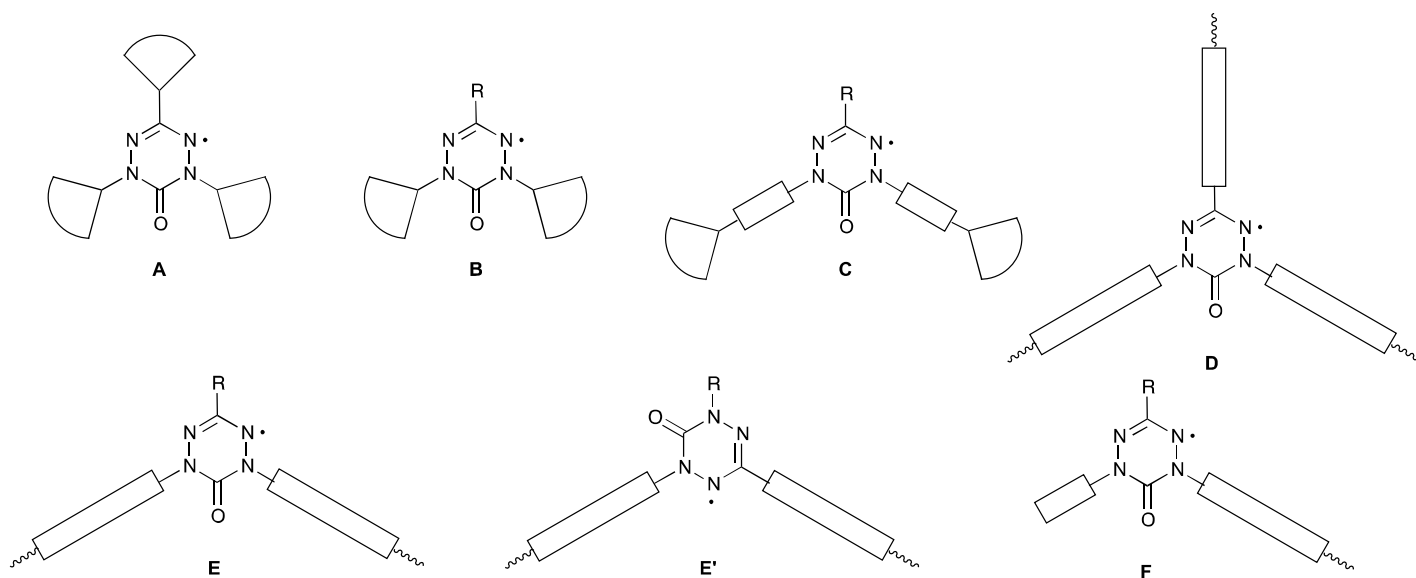

Chart I

General Synthesis

Structures shown in Chart I are conveniently accessible using the Milcent method[14] in a three-step process presented in Scheme 1. Thus, hydrazines **II** are converted to hydrazones **III**, which are reacted with triphosgene to give carbamoyl chloride **IV**. After isolation and purification, the chlorides are reacted with another hydrazine **II**. The resulting tetrazanes **V** are purified and oxidized, typically with $NaIO_4$ under PTC conditions or with PbO_2, to give radicals **I** in 10%–50% typical overall yields. This method allows for a convenient differentiation of the substituents.
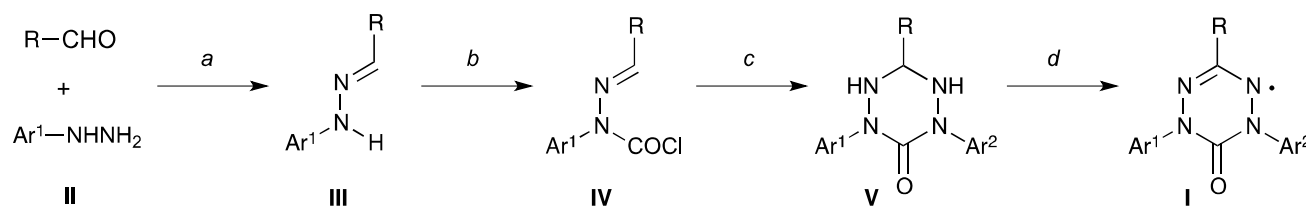
Scheme 1. Reagents and conditions: (a) EtOH, cat. AcOH, reflux; (b) $CO(OCCl_3)_2$, pyridine, CH_2Cl_2, rt; (c) Ar^2NHNH_2 (**II**), Et_3N, benzene, 50 °C; (d) PbO_2, Na_2CO_3, Toluene/MeCN or $NaIO_4$, Na_2CO_3 (0.5 M), $[Bu_4N]^+Br^-$ (cat.), CH_2Cl_2.

Alternatively, symmetrically substituted derivatives **I**, can be obtained by condensation of the N,N'-diarylcarbohydrazide **VI** with appropriate aldehyde R-CHO followed by oxidation of the resulting tetrazane **V** (Scheme 2).[30,31] The hydrazides **VI** are conveniently obtained by arylation of carbohydrazide (**VII**) with Ar-I in the presence of Cu-phenanthroline complex.[31]
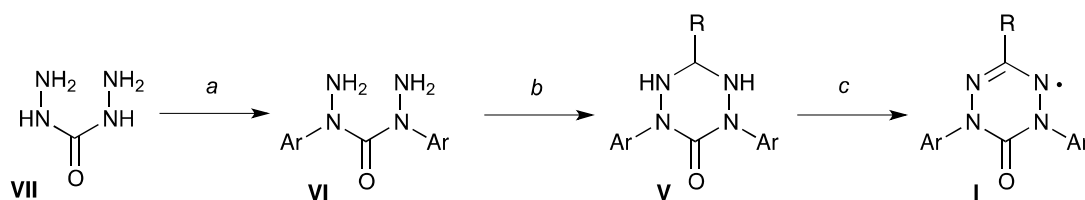
Scheme 2. Reagents and conditions: (a) ArI, CuI, 1,10-phenanthroline, K_3PO_4, DMF, 90 °C; (b) RCHO, EtOH, cat. acid; (c) PbO_2, Na_2CO_3, Toluene/MeCN or $NaIO_4$, Na_2CO_3 0.5 M, $[Bu_4N]^+Br^-$ (cat.), CH_2Cl_2.

Modification of functional groups and incorporation of the verdazyl system into more complex molecular architectures is possible through functional group transformations[13] in the presence of unpaired electrons (Scheme 3). In the context of formation of liquid crystalline derivatives, the most useful transformation is esterification of the phenolic functionality (X = OH → X' = OCOR). Unfortunately, neither *O*-alkylation of the phenols nor Pd-catalyzed C–C coupling reactions of *N*–(haloaryl) derivatives lead to the desired products.[13] It was demonstrated, however, that the C(3)–(haloaryl) derivatives of 6-oxoverdazyl undergo an efficient Suzuki–Miyaura coupling reaction.[32]
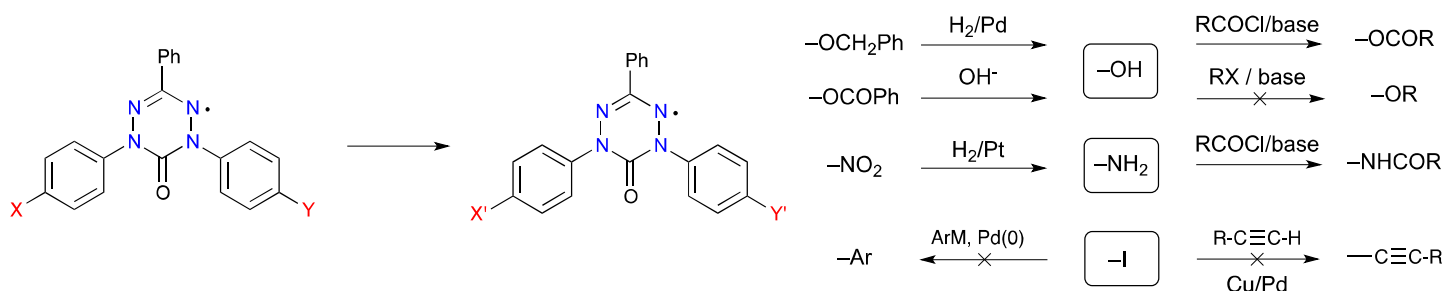
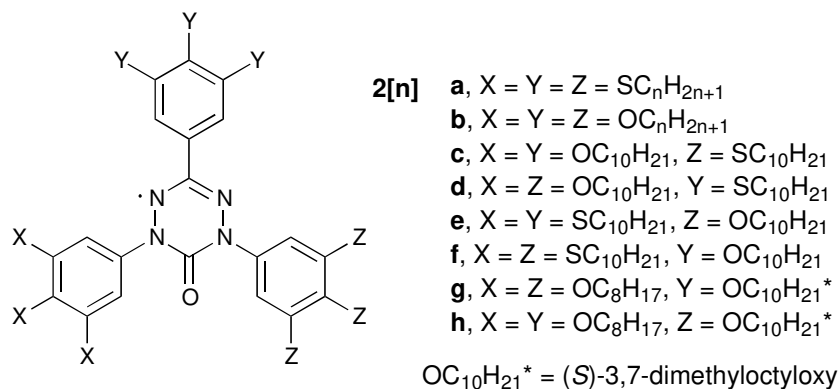**Scheme 3.** Functional group transformations (X →X' and Y →Y') in derivatives of 3-phenyl-6-oxoverdazyl.[13]

Molecular Materials and Liquid Crystalline Behavior

Disc-like derivatives type A

Substitution of the 6-oxoverdazyl with three wedge-shaped groups (3,4,5-trisubstituted phenyl groups) induced mesogenic behavior and derivatives **2[n]** exhibited columnar phases (Figure 7). Two derivatives with fewer total number of alkyl groups (3,4-disubstituted phenyl groups) did not form liquid crystalline phases, presumably due to low density of the alkyl chains in the molecular disk (see also ref.[33]).

2[n]	
a,	$X = Y = Z = SC_nH_{2n+1}$
b,	$X = Y = Z = OC_nH_{2n+1}$
c,	$X = Y = OC_{10}H_{21}, Z = SC_{10}H_{21}$
d,	$X = Z = OC_{10}H_{21}, Y = SC_{10}H_{21}$
e,	$X = Y = SC_{10}H_{21}, Z = OC_{10}H_{21}$
f,	$X = Z = SC_{10}H_{21}, Y = OC_{10}H_{21}$
g,	$X = Z = OC_8H_{17}, Y = OC_{10}H_{21}*$
h,	$X = Y = OC_8H_{17}, Z = OC_{10}H_{21}*$

$OC_{10}H_{21}* = (S)$-3,7-dimethyloctyloxy

**Figure 7.** Molecular structures of derivatives **2[n]**.

Thermal analysis indicated that lower homologues of **2a[n]** (n = 6, 8, 10) containing a total of nine alkylsulfanyl groups exhibit a novel 3D columnar hexagonal phase (*Col*$_{h(3D)}$, Table 1, Figure 8a), according to powder XRD analysis.[34,35] Only the shortest homologue, **2a[6]**, showed an enantiotropic phase, while two higher form monotropic mesophases and **2a[12]** do not exhibit liquid crystalline behavior. Replacement of the sulfur atoms in **2a[n]** with oxygen in **2b[n]** induced a broad range columnar hexagonal ordered phase (*Col*$_{h(o)}$, Figure 8b) with significantly higher clearing temperatures.[16] The correlation length in such columns is significant (210 Å at 110 °C for **2b[10]**), which is related to the observed pronounced thermochromism.[16] Interestingly, neither of the two investigated compounds, **2b[8]** and **2b[10]**, crystalizes, although the latter undergoes a phase transition at 20 °C to a *Col*$_{h(o)}$' phase, a close analogue of *Col*$_{h(o)}$ with the double size cell unit.

Brief experiments demonstrated that the two phases, *Col*$_{h(3D)}$ and *Col*$_{h(o)}$, formed by series **2a[n]** and **2b[n]**, respectively, are immiscible. Hoping for an unusual phase behavior of such a mixed system, a series of derivatives **2c[10] – 2f[10]** containing both types of substituents, 3,4,5-tridecylsulfanylphenyl and 3,4,5-tridecyloxyphenyl, was prepared.[36] Thermal analysis demonstrated that replacement of any of the 3,4,5-tridecyloxyphenyl substituents in **2b[10]** eliminates the order *Col*$_{h(o)}$ phase in favor of a *Col*$_h$ and lower isotropization temperature. In contrast, replacement of one of the 3,4,5-tridecylsulfanylphenyl groups in **2a[10]** increases stability of the *Col*$_{h(3D)}$ phase, and the largest increase is observed for derivative **2f[10]**, in which the substituent is modified at the C(3) position of the verdazyl ring. Interestingly, derivative **2d[10]** exhibits a dual polymorphism, *Col*$_{h(3D)}$ and *Col*$_h$ phases, demonstrating a higher degree of molecular organization in the former phase.

Table 1. Transition temperatures ($^{\circ}$C) for **2[n]**[a]

2[n]	n	Transition temperatures	lit
a	6	Cr 39 *Col*$_{h(3D)}$ 50 I	[b]
	8	Cr 62 (*Col*$_{h(3D)}$ 60) I	[b]
	10	Cr 62 (*Col*$_{h(3D)}$ 55) I	[b]
	12	Cr 63 I	[b]
b	8	Cr < 25 *Col*$_{h(o)}$ 127 I	[c]
	10	Cr < 0 *Col*$_{h(o)}$' 20 *Col*$_{h(o)}$ 121 I	[c]
c	10	Cr 47 *Col*$_{h}$ 91 I	[d]
d	10	Cr 57 *Col*$_{h(3D)}$ 78 *Col*$_{h}$ 80 I	[d]
e	10	Cr 51 *Col*$_{h(3D)}$ 67 I	[d]
f	10	Cr 49 *Col*$_{h(3D)}$ 102 I	[d]
g	8	Cr < 25 *Col*$_{h(o)}$ 73 I	[e]
h	8	Cr < 20 *Col*$_{h(o)}$ 67 *Col*$_{h}$ 78 I	[e]

[a] Determined by DSC in the heating mode (5 K min^{-1}): Cr = crystalline; *Col*$_{h}$ = columnar hexagonal; *Col*$_{h(3D)}$ = columnar hexagonal 3D; *Col*$_{h(o)}$ and *Col*$_{h(o)}$' = columnar hexagonal ordered; I = isotropic. [b] Ref.[34,35]. [c] Ref.[16]. [d] Ref. [36]. [e] Ref. [37].

a　　　　　　　　　　b　　　　　　　　　　c
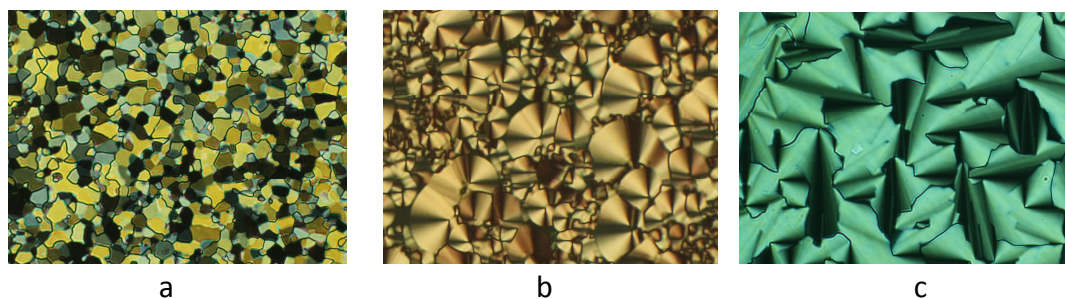
Figure 8. Optical textures of *Col*$_{h(3D)}$ phase in **2a[8]** (a), *Col*$_{h(o)}$ phase in **2b[10]** (b), and *Col*$_{h}$ phase in **2h[8]** (c).

The induction of homochiral helical columnar structures in series **2[n]** was investigated using (*S*)-3,7-dimethyloctyloxy substituents.[37] Unfortunately, no evidence was found supporting the helical organization of the molecules in columns, and only a typical signature for *Col*$_{h(o)}$ and *Col*$_{h}$ phases was observed. The replacement of the 3,4,5-trioctyloxyphenyl substituent in **2b[8]** with 3,4,5-tris((*S*)-3,7-dimethyloctyloxy)phenyl resulted in a significant decrease of mesophase stability in **2g[8]** and **2h[8]** due to the alkyl chain branching. Interestingly, the effect is stronger when position C(3) is modified in **2g[8]**, demonstrating the apparently dominant role of this aryl substituent in phase stabilization.

The observed generally higher stability of columnar phases for the derivatives with the trialkoxyphenyl substituents relative to the analogous trialkylsulfanylphenyl derivatives is related to conformational properties of the peripheral substituents: in contrast to the alkylsulfanyl groups, the alkoxy groups prefer coplanar orientation with the benzene ring, which gives rise to more anisometric molecules (Figure 9).[35]
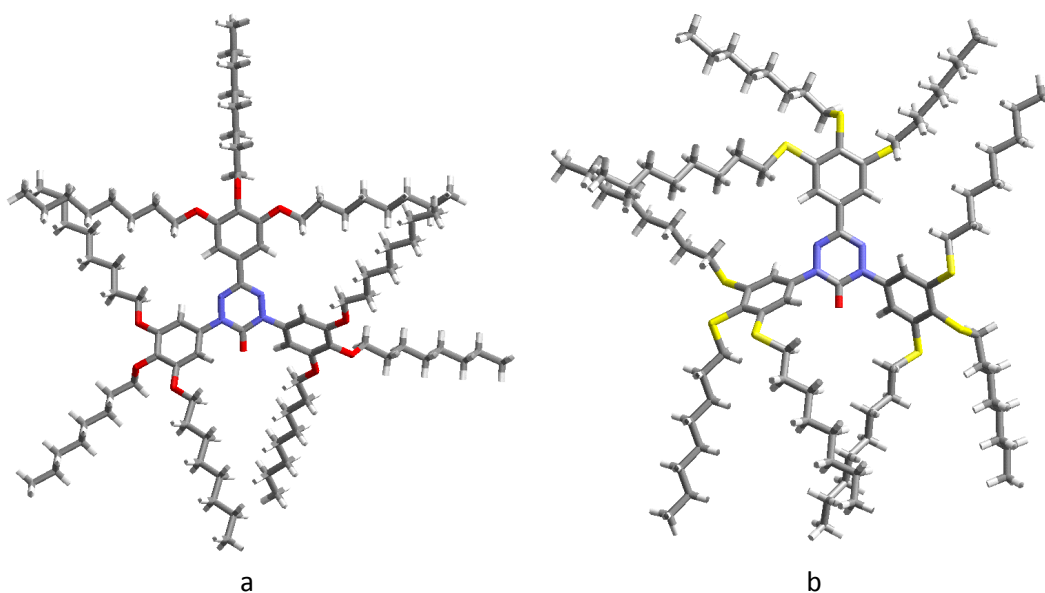
Figure 9. Molecular structures of **2b[8]** (a) and **2a[8]** (b) optimized with the UFF algorithm. Alkyl chains are set in the all-*trans* conformation.

The conformational properties of the phenyl substituents connected to the central 6-oxoverdazyl core in derivatives **2[n]** also affect the phase stability. Thus, steric interactions with the carbonyl group result in sizable dihedral angles between the aryl substituents in positions N(1) and N(5) and the heterocycle (Figures 5 and 9), which lower molecular anisometry and, consequently, decrease phase stability. Support for this notion is provided by a comparison of **2b[10]** with its planar 1,3,5-triazine analogue[38] **3[10]**, which indeed shows a 24 K higher *Col→Iso* transition temperature (Figure 10). Further comparison with planar boroxine[39] **4[10]** and propeller-like benzene[33] **5[10]** derivatives demonstrate that other factors, such as symmetry and the net dipole moment of the core, also play a role in stabilization of columnar mesophases.
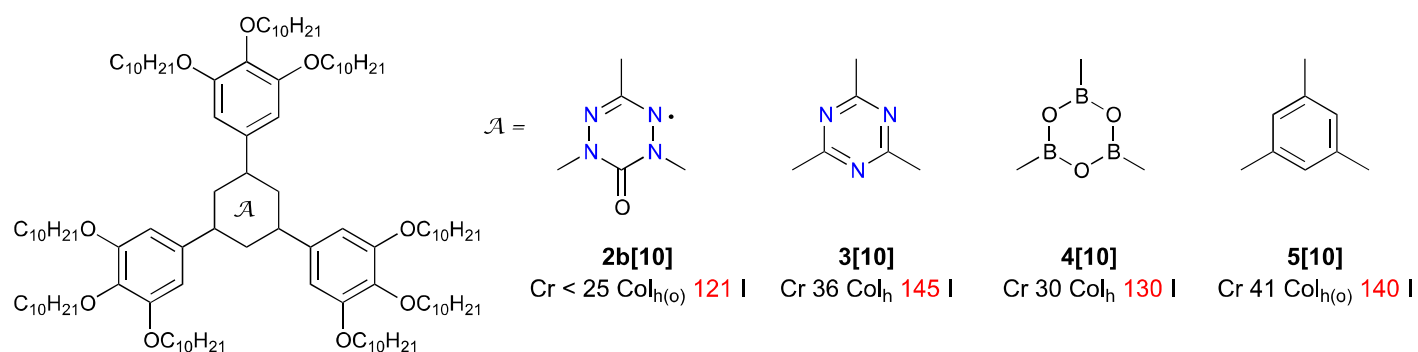
Figure 10. A comparison of the effect of the central ring on mesophase stability.

Half-disc derivatives type C

A replacement of a wedge-shaped substituent at the C(3) position in **2[n]** with a small group leads to half-disk structure **B** (Chart I), which has not been studied experimentally to date. Instead, the two remaining wedge-shaped groups in **B** were moved away from the 6-oxoverdazyl core using rigid spacers in derivatives of type **C** (Chart I). For testing this molecular architecture, 3,4-didodecyloxyphenyl and 3,4,5-tridodecyloxyphenyl

substituents were selected and connected with the core using either a short spacer in **6** and **7** or a long spacer in **8** and **9** (Figure 11). Unfortunately, none of these derivatives **6a** – **9a**, containing a small 2-thienyl group at the C(3) position, exhibited mesogenic behavior, even upon supercooling. Increasing of the number of dodecyloxy substituents from 2 in **6a** and **8a** to 3 in derivatives **7a** and **9a** resulted only in a decrease of the melting point (Table 2). Changing the substituent at the C(3) position from 2-thienyl in **7a** to 3-fluorophenyl in **7b** or trifluoromethyl in **7c** also failed to induce a liquid crystalline phase.
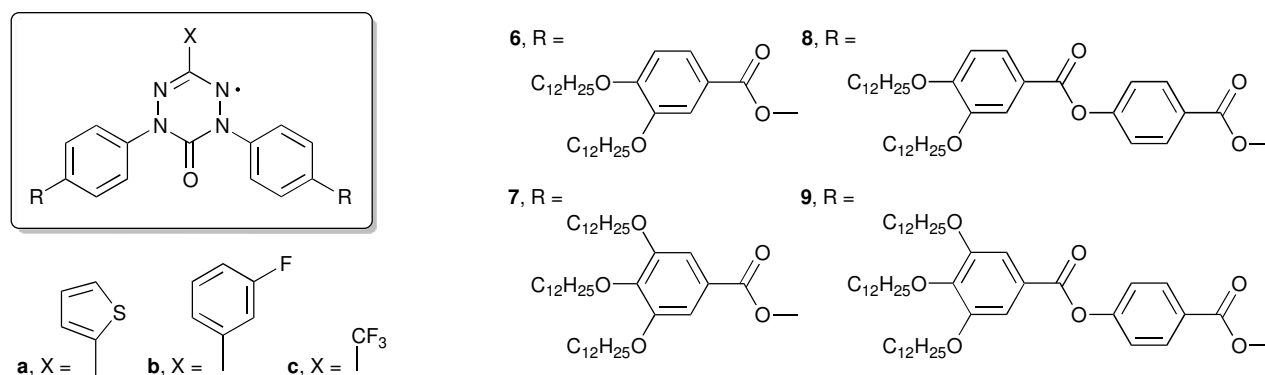
Figure 11. Molecular structures of derivatives **6 – 9**.

Table 2. Transition temperatures (^{o}C) for **6 – 9**[a]

Compound	Transition temperatures
6a	Cr 89 I
7a	Cr 81 I
7b	Cr 82 I
7c	Cr 52 I
8a	Cr 147 I
9a	Cr 113 I

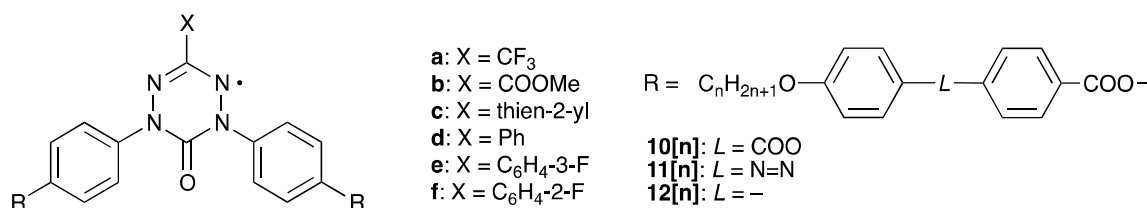[a] Determined by DSC (10 K min^{-1}) in the heating mode: Cr = crystalline; I = isotropic.

Star-like derivatives D
Verdazyl substituted derivatives with three rod-like groups containing one or two alkoxy chains in each (i.e. analogs of **6** with three long "arms" instead of two) have not been studied experimentally. On the basis of literature data for other such derivatives, discotic nematic phases (N$_D$) can be expected with low degree of molecular organization.[24] Such derivatives could conveniently be obtained from 1,3,5-tri(4-hydroxyphenyl)-6-oxoverdazyl.

Bent-core derivatives E and E'
Substitution of the 6-oxoverdazyl with two rod-like fragments leads to bent-core derivatives of type **E** and their isomers **E'** (Chart I). Initially symmetrical derivatives **E** containing a small polar CF$_3$ group in position C(3) were investigated (Figure 12). Thermal analysis of series **10a[n]** revealed an unusual polymorphism, not related to banana phases (Table 3).[40] The lower homologues **10a[8]**– **10a[12]** exhibit a nematic phase and a monotropic SmA phase was found in **10a[8]**. In contrast, higher homologs **10a[14]** and **10a[16]** exhibit a novel 3D tetragonal phase (*Tet*$_{(3D)}$, Figure 13a) and two distinct isotropic phases, I and I'. In order to study this

diverse behavior in this series and to shed more light on the nature of the I-I' transition, a 3:1 mixture of **10a[12]** and **10a[14]** was prepared which mimics the homologue **10a[12.5]**. Investigations demonstrated that the mixture exhibits both the nematic and tetragonal phases separated with a re-entrant isotropic phase (I_{re}) present also in the **10a[12]** homologue. The phase diagram in Figure 14 helps to visualize the relationship between the polymorphism of homologues and relates the I' phase in higher homologues with I_{re} in lower members of the series.

a: X = CF_3
b: X = COOMe
c: X = thien-2-yl
d: X = Ph
e: X = C_6H_4-3-F
f: X = C_6H_4-2-F

R = C_nH_{2n+1}O— ... —L— ... —COO—

10[n]: *L* = COO
11[n]: *L* = N=N
12[n]: *L* = –

Figure 12. Molecular structures of derivatives **10[n] – 12[n]**.

Table 3. Transition temperatures (°C) for **10a[n] – 12a[n]**[a]

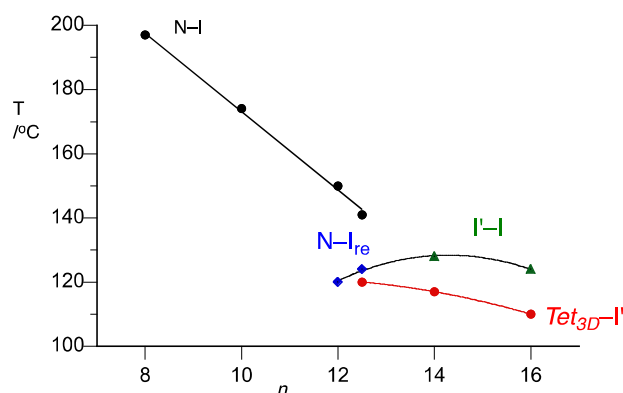| Compound	n	L	Transition temperatures
10a[n]	8	COO	Cr 150 (SmA 141)[b] N 197 I
	10	COO	Cr 140 N 174 I
	12	COO	Cr 133 (I_{re} 120)[b,c] N 150 I
	14	COO	Cr 98 Tet_{3D} 117 I' 128 I
	16	COO	Cr 84 Tet_{3D} 110 I' 124 I
11a[n]	12	N=N	Cr 137 Tet_{3D} 142 I' 151 I
12a[n]	12	–	Cr 122 Tet_{3D} 129 I' 140 I

[a] Cr = crystal; N = nematic, Sm = smectic, Tet_{3D} = tetragonal 3D; I and I' = isotropic. Recorded for fresh samples on heating. Data from ref.[40]. [b] Monotropic transition recorded on cooling. [c] Microscopic observation.

a   b
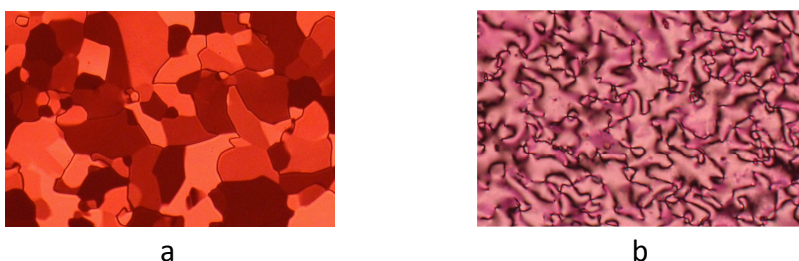
Figure 13. Optical textures of a $Tet_{(3D)}$ phase in **10a[14]** (a) and a nematic phase in **10e[12]** (b).

The role of the linking group *L* in the "arm" was briefly investigated using dodecyloxy derivatives (Figure 12). Thus, replacement of the COO group in **10a[12]** with an azo group N=N in **11a[12]** or removing it in derivative **12a[12]** resulted in elimination of the nematic phase and appearance of the tetragonal phase ($Tet_{(3D)}$) characteristic for higher homologs **10a[n]**.

Figure 14. N–I (black), N-I$_{re}$ (blue), Tet$_{3D}$ –I' (red) and I'-I (green) phase transition temperatures as a function of the alkyl chain length in **10a[n]**. The data point for "**10a[12.5]**" was obtained from a mixture of **10a[12]** and **10a[14]**. Lines are guide for the eye. Data from ref.[40]

The effect of the "head" group at the C(3) position on mesogenic properties was investigated in the series **10a[12]–10f[12]** (Figure 12).[41] Thus, replacing the CF_3 group in **10a[12]** with another small polar group, COOMe, in **10b[12]** increased stability of the nematic phase by 11 K (Table 4). Substituting aryl groups for CF_3 increased melting points of compounds **10c[12]** – **10f[12]** and only *m*-fluorophenyl derivative **10e[12]** exhibited a monotropic nematic phase (Figure 13b). Extending the *n*-dodecyl alkyl chain to *n*-$C_{16}H_{33}$ in **10c[16]** and **10d[16]** had surprisingly little effect on the melting point and did not induce any mesogenic behavior.

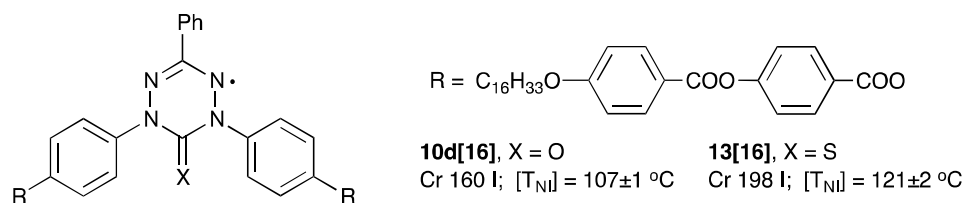**Table 4.** Transition temperatures (°C) for **10a[n] – 10f[n]**[a]

Compound 10	X	Transition temperatures	Virtual transition temperatures	
			[T_{NI}]	[T_{NIre}]
a[12]	CF_3	Cr 133 (I$_{re}$ 120)[c] N 150 I	–	–
b[12]	COOMe	Cr 139 N 161 I[d]	231	[e]
c[12]	Thien-2yl	Cr 153 I	138	136
d[12]	Ph	Cr 157 I	163	139
e[12]	C_6H_4-3-F	Cr 177 (N 169)[c] I	194	110
f[12]	C_6H_4-2-F	Cr 155 I	82	144
c[16]	Thien-2yl	Cr 149 I	91	150
d[16]	Ph	Cr 160 I	102	140
			107±1[f]	132±1[g]

[a] Cr = crystal, N = nematic, I and I$_{re}$ = isotropic. Data from ref.[41] [b] Extrapolated from ~10 mol% solutions in **10a[12]**. [c] Monotropic transition. [d] Decomposition. [e] Not observed. [f] Linear extrapolation from 3 solutions. Ref.[42] [g] Nonlinear extrapolation from 3 solutions. Ref.[42]

In order to compare effectiveness of the substituent at the C(3) position in mesophase formation, virtual N-I transition temperatures for **10b[12]–10f[12]** were extrapolated from 10 mol% binary mixtures with the CF_3 derivative **10a[12]**. Results in Table 4 show that the nematic phase stability follows the order: COOMe > *m*-FC_6H_4 > Ph > 2-thienyl > *o*-FC_6H_4. Higher stability of the nematic phase observed for the *m*-FC_6H_4 derivative **10e[12]** relative to C(3)-Ph derivative **10d[12]** is presumably related to the polarity of the substituent. Extending the alkyl chain length destabilizes the mesophase of the host.

Interestingly, the transition temperature to the re-entrant isotropic phase follows a different order and in general, the lower stabilization of the nematic phase, the higher temperatures for the appearance of the I_{re} phase.

For comparison purposes, one bent-core derivative of 6-thioxoverdazyl, compound **13[16]**, was prepared as a direct sulfur analogue of **10d[16]** (Figure 15).[42] Analysis demonstrated that neither derivative forms a mesophase, and **13[16]** has higher melting point by nearly 40 K than the oxygen analogue. Binary mixtures with **10a[12]** revealed also a higher, by 14 K, extrapolated virtual N-I transition temperature for the sulfur derivative, presumably due to higher polarizability of the S atom and over twice higher dipole moment of the 6-thioxoverdazyl core (1.81 D *vrs* 0.77 D calculated in vacuum at the UB3LYP/6-31G(2d,p) level of theory for the model 1,3,5-triphenyl derivatives). It should be noted that access to such thioxo derivatives is hampered by synthetic problems and low yields of the 6-thioxoverdazyl ring formation.

R = $C_{16}H_{33}O$—⬡—COO—⬡—COO

10d[16], X = O   **13[16]**, X = S
Cr 160 I; [T_{NI}] = 107±1 °C   Cr 198 I; [T_{NI}] = 121±2 °C

Figure 15. A comparison of melting points and virtual N-I transition temperatures (linear extrapolation) for two chalcogen analogues obtained from three solutions in **10a[12]** host. Ref .[42]

Induction of mesogenic behavior in derivatives of 6-oxoverdazyl with a large steroid substituent was briefly investigated. For this purpose two symmetrical derivatives **14a** and **14b** containing the saturated cholestanyl fragment were prepared (Figure 16). The saturated steroid moiety was used to avoid possible reactions of the radical center with the double bond. Unfortunately neither compound showed the expected cholesteric phase, and the high melting points, essentially above thermal stability of the verdazyl, discouraged further structural modifications to induce mesogenic behavior.

R =

14   a, X = CF$_3$: Cr 206 I
       b, X = Ph: Cr 228 dec I
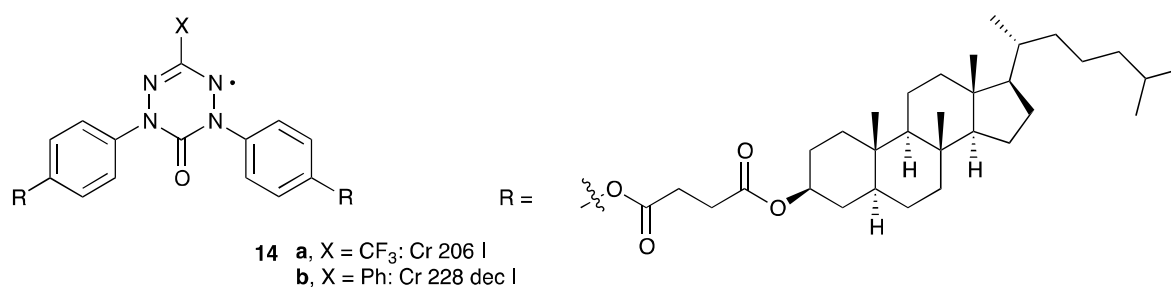
Figure 16. Structure and transition temperatures of cholestanyl derivatives of 6-oxoverdazyl **14**.

Lamellar phases in bent-core derivatives of 6-oxoverdazyl were induced using partially fluorinated terminal alkoxy substituents.[43] Thermal analysis of series **15[m,n]** (Figure 17) showed that all diesters form smectic phases with high clearing temperatures (Table 5). In general: the higher the F/H ratio, the higher SmA–I transition temperature. This is in agreement with general trends[44] and due to the increasing length of the rigid fluorocarbon segment. Compounds with the CF$_3$ group at the C(3) position exhibit enantiotropic SmA and monotropic SmC phases (Figure 18), while derivatives with an aryl substituent form only a broad range enantiotropic SmA phase. Interestingly, analysis of series **15a[6,6]** − **15d[6,6]** demonstrates that the effect of

the C(3) substituent on SmA phase stability is different than in series **10b[12]** – **10f[12]** and follows the order: 2-thienyl > *m*-FC$_6$H$_4$ > Ph > CF$_3$. The broad-range and high thermal stability of the thienyl derivatives **15b[m,n]** is of relevance to the development of organic photoconductors.

15[m,n]

a: X = CF$_3$
b: X = thien-2-yl
c: X = Ph
d: X = C$_6$H$_4$-3-F

R = C$_m$F$_{2m+1}$(CH$_2$)$_n$O—⟨ ⟩—COO
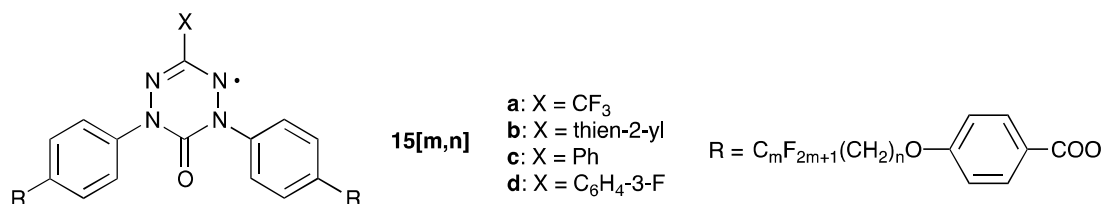
Figure 17. Molecular structures of derivatives **15[m,n]**.

Table 5. Transition temperatures (^{o}C) for **15[m,n]**[a]

| Compound 15	(CF$_2$)$_m$	(CH$_2$)$_n$	Transition temperatures
a[6,4]	6	4	Cr 156 I
a[8,4]	8	4	Cr 127 (SmC 108)[b] SmA 150 I
a[10,4]	10	4	Cr 144 (SmC 137)[b] SmA 183 I
a[6,6]	6	6	Cr 132 (SmC 74 SmA 91)[b] I
a[8,6]	8	6	Cr 124 (SmC 116)[b] SmA 149 I
b[8,4]	8	4	Cr 129 SmA 245 I[c]
b[10,4]	10	4	Cr 136 SmA ~220 I[c]
b[6,6]	6	6	Cr 107 SmA 197 I[c]
c[6,6]	6	6	Cr 135 SmA 183 I
d[6,6]	6	6	Cr 147 SmA 192 I

[a] Cr = crystal, SmA = smectic A, SmC = smectic C, I = isotropic. Data from ref.[43]. [b] Monotropic transition. [c] Decomposition.

a   b
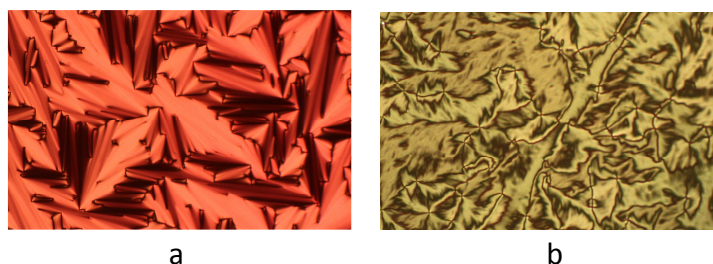
Figure 18. Optical textures of smectic A (a) and smectic C phases in **15a[6,6]** (b).

In parallel with investigation of symmetric bent-core derivatives **E**, we initiated work towards isomeric compounds of structure **E'** (Chart I). Preliminary results demonstrate lower melting points and the appearance of a monotropic SmA phase,[45] as shown for the pair **10d[12]** and **16[12]** in Figure 19. The observed lower stability of the crystal phase for the latter compound is presumably related to the lower symmetry of derivatives **E'**. This finding indicates a promising approach to materials with low melting points; it offers however a limited choice of substituents at the N(5) position dictated by the chemical stability of the verdazyls and accessibility of the corresponding hydrazines.
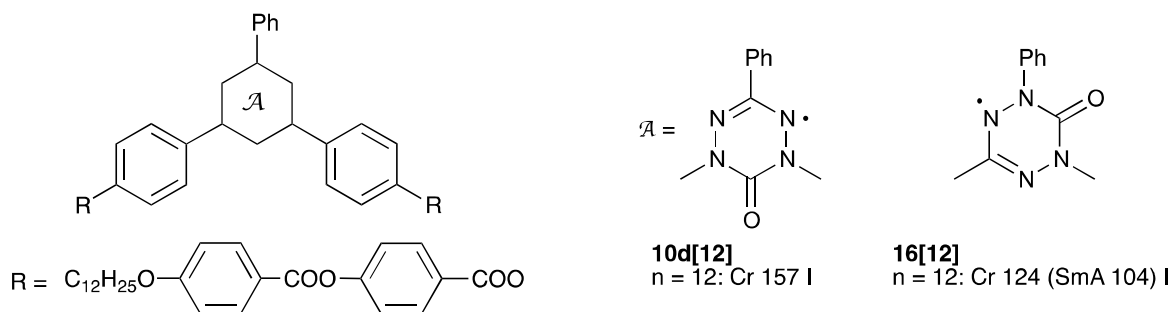
Figure 19. A comparison of thermal properties of an isomeric pair of compounds. Ref. [45]

Hockey-stick derivatives F

Truncation of one of the "arms" and removal of the alkoxy group in the bent-core derivatives **E** leads to hokey-stick architecture **F** (Chart I). Thus, shortening of one "arm" in series **10a[n]** gives series **17[n]** and their close analogues **18 – 20** (Figure 20, Table 6).[46]
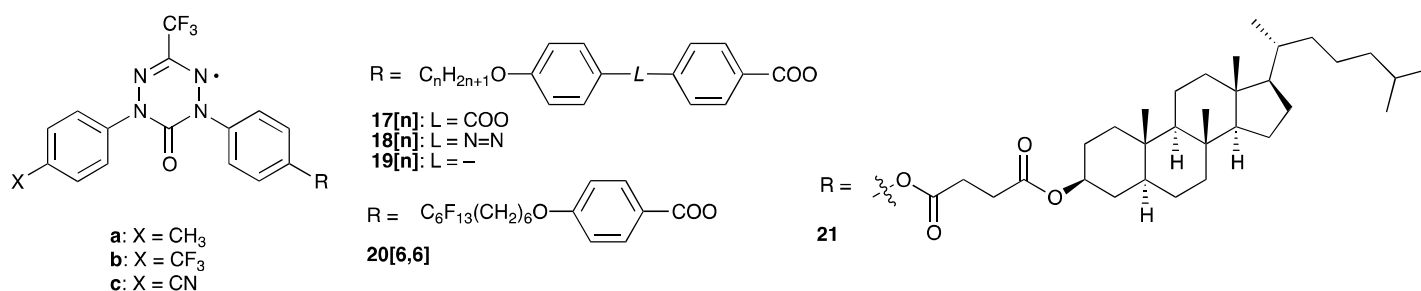
Figure 20. Molecular structures of derivatives **17[n] – 21**.

Table 6. Transition temperatures (^{o}C) for **17[n] – 21**[a]

Compound	X	Transition temperatures
17a[12]	CH$_3$	Cr 138 I
17a[14]		Cr 128 I
17a[16]		Cr 121 I
17b[12]	CF$_3$	Cr 129 I
17c[8]	CN	Cr 98 N 133 I
17c[10]		Cr 127 (N 115)[b] I
17c[12]		Cr 123 (N 102)[b] I
18c[12]		Cr 152 (N 88)[b] I
19c[12]	CN	Cr 116 I
20c[6,6]	CN	Cr 146 I
21a	CH$_3$	Cr 133 I
21c	CN	Cr 93 I

[a] Cr = crystal, N = nematic, I = isotropic. Data from ref [46]. [b] Monotropic transition.

Analysis of data in Table 6 indicates that derivatives **17a[n]** with a relatively small methyl terminal substituent in the short arm (X = CH$_3$) do not form liquid crystalline phases even upon elongation of the

terminal chain to n-$C_{16}H_{33}$ in **17a[16]**. Replacement of the CH_3 group in **17a[12]** with CF_3 only lowers the melting point of **17b[12]** by 9 K without induction of a mesophase. Finally, placing the cyano group, a strong nematic phase promoter,[18] in the short "arm" leads to the appearance of a monotropic nematic phase in series **17c[n]**. Interestingly, thermal stability of the nematic phase decreases with increasing alkyl chain length.

To test further structural effects on mesophase stability, the linking group L and also the character of terminal substituents were modified (Figure 20). Thus, replacement of the ester group, L = COO, in **17c[12]** with an azo (L = N=N) in **18c[12]** markedly increased the melting point and suppressed the nematic phase by 14 K. Removing of the ester group (L = −) in **19c[12]** eliminated the mesogenic behavior.

Finally, using a partially fluorinated C_{12} alkyl chain in **20c[6,6]** or a large cholestanyl fragment in **21** did not induce the formation of a liquid crystalline phase. In the former case, only a significant increase in the melting point was observed.

Magnetic Behavior

Magnetic interactions in liquid crystalline radicals can be probed either by measuring magnetization of the sample with a SQUID magnetometer or by following the peak width and the g value as a function of temperature using EPR spectroscopy. The former measures bulk magnetic properties and typically has the upper limit of 400 K, while EPR spectroscopy probes local magnetic interactions.

Magnetization studies of four discotic **2[n]** and one bent-core (**10a[16]**) derivatives as a function of temperature revealed weakly interacting spins. In derivatives **2a[8]**, **2d[10]**, and **10a[16]** no abrupt changes of magnetic susceptibility at phase transitions were detected (Table 7). Instead a smooth decrease of the $\chi_p \bullet T$ product was observed upon cooling from the isotropic phase to 2K due to gradually increasing antiferromagnetic interactions. Only in samples **2b[8]**[16] and **2h[8]**[37] was a decrease of magnetization by ~5% upon formation of the more organized *Col*$_{h(o)}$ phase observed (Figure 21). Thus, the results indicate that the substituents prevent effective intermolecular close π–π contacts, and the unpaired electrons remain largely isolated in either the rigid or fluid phases.
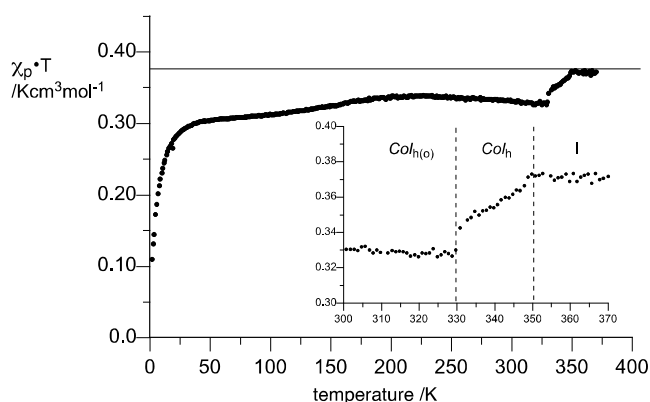
Figure 21. $\chi_p \bullet T$ *vrs* T plot for **2h[8]** measured on cooling at 200 Oe. The horizontal line marks the value 0.375 cm^3 K mol^{-1} for an ideal paramagnet. The inset shows the high-temperature portion of the plot with marked phase transition temperatures.[37]

Table 7. Results of magnetic susceptibility (χ_p) studies for selected derivatives[a]

Compound	Phase type	Comments	Lit
2a[8]	*Col*$_{h(3D)}$	no effect of phase transition on $\chi_p \bullet T$	a
2b[8]	*Col*$_{h(o)}$	5% decrease of $\chi_p \bullet T$ upon *Iso* → *Col*$_{h(o)}$ transition	b
2d[10]	*Col*$_{h(3D)}$, *Col*$_h$	no effect of phase transition on $\chi_p \bullet T$	c
2h[8]	*Col*$_{h(o)}$, *Col*$_h$	5% decrease of $\chi_p \bullet T$ upon *Iso* → *Col*$_{h(o)}$ transition	d
10a[16]	Tet$_{(3D)}$	no effect of phase transition on $\chi_p \bullet T$	e

[a] Ref.[34]. [b] Ref.[16]. [c] Ref.[36]. [d] Ref.[37]. [e] Ref.[40].

Charge Mobility

Mobility of photogenerated charges and the photo-current are important parameters of photovoltaic materials. Time-of-flight (TOF) measurements[47] conducted for three discotic derivatives, **2a[8]**, **2b[8]**, and **2d[10]**, found positive charge carrier (hole) mobility (μ_h) in fast-cooled, unaligned multidomain samples (Table 8). In all three derivatives, hole mobility μ_h in the columnar phase was in a range of $1-3 \times 10^{-3}$ cm^{2}V^{-1}s^{-1} (Figure 22), which is typical for columnar mesophases of closed-shell compounds ($10^{-4}-10^{-1}$ cm^{2}V^{-1}s^{-1}).[48,49] Charge photogeneration was more efficient for alkylsulfanyl derivative **2a[8]** than for trialkoxyphenyl derivatives **2b[8]** and **2d[10]**.[36] For example, for **2b[8]** photocurrent was only 6.0×10^{-13} S cm^{-1} at 90 ^{o}C, comparable with the dark current (4.0×10^{-13} S cm^{-1} at 90 ^{o}C), and no photoconductivity was detected in the isotropic phase.[16]

Table 8. Mobility (μ_h) of photogenerated positive charges.

Compound	Phase type	μ_h cm^{2}V^{-1}s^{-1}	T /^{o}C	Comments	Lit
2a[8]	*Col*$_{h(3D)}$	1.52×10^{-3}	40	$E_a = 0.06 \pm 0.01$ eV	a
2b[8]	*Col*$_{h(o)}$	3.3×10^{-3}	60	low current	b
2d[10]	*Col*$_{h(3D)}$, *Col*$_h$	–	c	very low current	d
10a[16]	Tet$_{(3D)}$	0.9×10^{-3}	90	$E_a = 0.03 \pm 0.01$ eV	e
15a[8,4]	SmA	–	130	no current	f

[a] Ref.[34]. [b] Ref.[16]. [c] Temperature range 30-80 ^{o}C. [d] Ref.[36]. [e] Ref.[40]. [f] Ref.[43].
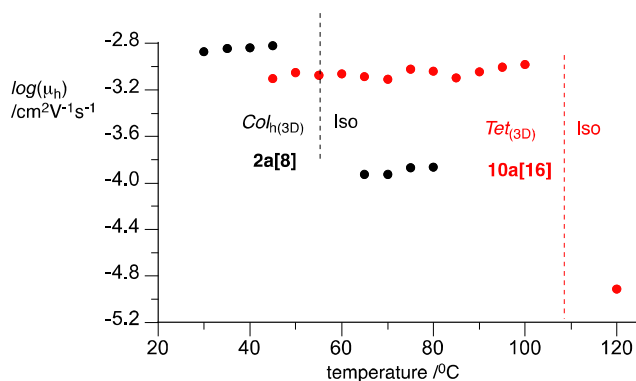
Figure 22. The temperature dependence of positive carrier mobility obtained by the TOF method for **2a[8]** (black) and **10a[16]** (red). Electric field strength 40 kV cm^{-1}. Ref.[16,40].

In contrast to the discotic derivatives, ambipolar charge transport was detected in the Tet$_{(3D)}$ phase of bent-core derivative **10a[16]** demonstrating a bicontinuous nature of this phase.[40] On the other hand, no photocurrent was detected in a SmA phase of another bent-core derivative **15a[8,4]**.[43] The Arrhenius analysis of μ_h for **2a[8]** and **10a[16]** at several temperatures show low activation energy for, e.g. E_a = 0.06±0.01 eV for **2a[8]**,[34] which is consistent with a hopping transport mechanism.

Summary and Conclusions

Analysis of the 6-oxoverdazyl structure shows that a number of molecular architectures suitable for induction of liquid crystalline phases can be envisioned. The design of such derivatives is limited to (Het)aryl groups and small substituents without α-hydrogen atoms to ensure their sufficient chemical stability. Another limitation is imposed by the availability of appropriate hydrazines **II** or their equivalents (e.g. *N*-arylated carbohydrazides **VI**).

Out of seven presented molecular architectures, five have been tested experimentally and four exhibited liquid crystalline behavior; columnar and calamitic phases were observed, although, despite efforts, no banana phases with higher molecular organizations were found so far. Investigation revealed unusual polymorphism, including the existence of two isotropic phases and a re-entrant isotropic phase in some bent-core derivatives, and led to the discovery of two new liquid crystalline phases (*Col$_{h(3D)}$* and Tet$_{(3D)}$). Initial results for series **E'** warrant further investigation of the impact of "broken symmetry" on thermal behavior of bent-core mesogens: in comparison with analogues **E**, they appear to have lower melting points, which is favorable for mesophase formation. Unfortunately, the choice of the small substituent in position N(5) is limited.

Between the remaining two molecular architectures, **B** and **D**, particularly attractive is the former, which is expected to lead to columnar phases with possibly new molecular organization and favorable photovoltaic properties. Also investigation of the isomeric pairs **B** and **B'**, and also **E** and **E'** would provide important insight into the role of the orientation of the molecular dipole moment on mesogenic behavior.

Magnetic susceptibility measurements demonstrated that electron spins in mesogenic 6-oxoverdazyls are largely isolated in all phases. These materials show weak, at best, dependence of magnetic properties on the phase structure and gradual increase of antiferromagnetic interactions upon cooling to 2 K.

Photoconductivity measurements in discotic phases of 6-oxoverdazyls revealed hole mobility μ_h on the order 10^{-3} cm^{2}V^{-1}s^{-1}, which is typical for closed-shell discotic derivatives. Typically only mobility of positive charges (holes) was observed, although in the *Tet*$_{(3D)}$ phase of bent-core mesogens ambipolar charge transport was detected.

The presented analysis shows a wealth of molecular architectures that can be derived from 6-oxoverdazyls conducive to the formation of partially organized paramagnetic fluids. Results obtained thus far constitute a significant contribution to the field of liquid crystal research, and indicate directions for fine-tuning of properties and further development of soft materials with a unique combination of properties.

Experimental Section

General. Reactions were typically performed in flame-dried flasks. Solvents and reagents were added by syringe. Dichloromethane was dried over CaH$_2$ and stored under inert atmosphere. Other reagents and solvents were purchased and used as received without further purification. Products were purified by flash chromatography on silica gel (230–400 mesh, Merck or Fluka). Unless stated otherwise, yields refer to analytically pure samples. NMR spectra of non-radical substrates were recorded with Bruker AVIII 600

instrument. IR spectra were measured with a FTIR NEXUS spectrometer (as KBr pellets). EI-MS spectra were performed with a Finnigan MAT-95 instrument. Positive ion MALDI mass spectra were recorded on the Voyager-Elite (PerSeptive Biosystems Inc., Framingham, MA, USA) instrument in reflector mode. A 10 mg mL^{-1} solution of 2-amino-5-nitropyridine in 50% acetonitrile was used as a matrix. Optical rotations were determined with an Anton Paar MCP 500 polarimeter at the temperatures indicated. Elemental analyses were obtained with a Vario EL III (Elementar Analysensysteme GmbH) instrument. Melting points were determined in capillaries with a MEL-TEMP II apparatus (Aldrich) or with a POM (Opta-Tech) and are uncorrected. Thermal measurements were done on a differential scanning calorimeter Mettler DSC-1 (STAR System, Mettler Toledo, Columbus, OH, USA) at a typical scanning rate of 10 Kmin^{-1}.

Preparation of acid chlorides. To a solution of the appropriate carboxylic acid[50,51] (0.57 mmol) and excess thionyl chloride (1.71 mmol; 0.12 mL) in dry CH_2Cl_2 (5 mL) 3 drops of dry DMF were added, and the mixture was stirred overnight under an atmosphere of Ar. The unconsumed thionyl chloride was removed under vacuum, and the resulting solid was dissolved in dry CH_2Cl_2. The solvent was evaporated in vacuo, and the procedure was repeated 2-3 times. The crude acyl chloride was dried under vacuum until no more odor of thionyl chloride was detected, and it was used for the next step without further purification.

General procedure for the synthesis of 6-oxoverdazyls esters and diesters 6-9, 14, 20, and 21
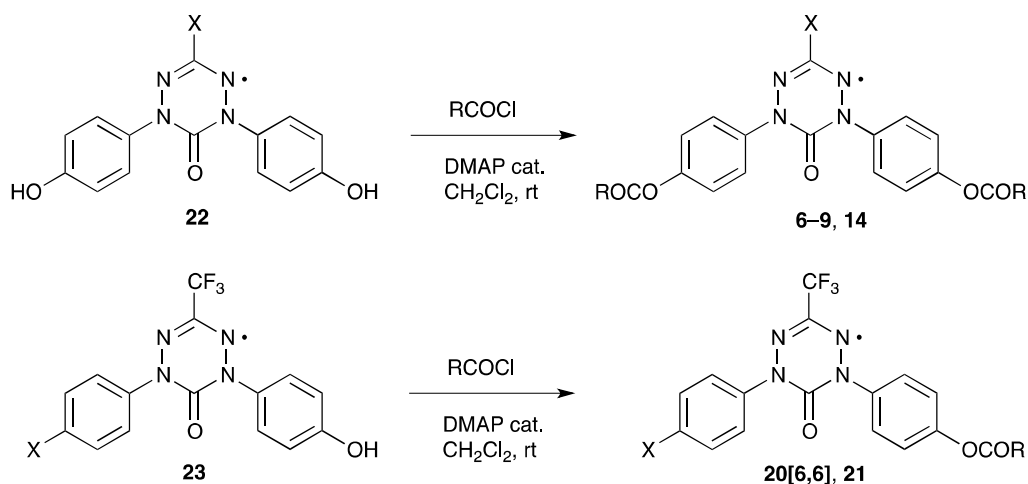
A mixture of the appropriate 6-oxoverdazyl diphenol **22** [40,41] or monophenol **23** [46] (0.20 mmol) and freshly prepared acid chloride (1.2 equiv. per OH group) in dry CH_2Cl_2 (10 mL) containing DMAP (73 mg, 0.60 mmol) was stirred at room temperature until the starting material was fully consumed (typically 20-40 min). The mixture was quenched with H_2O, diluted with CH_2Cl_2 and the organic layer was washed with 2% HCl (10 mL), 5% aq. $NaHCO_3$ (10 mL), and with H_2O (3 × 25 mL). The mixture was dried ($MgSO_4$), filtered, and the solvents were removed under reduced pressure. If not stated otherwise, the resulting crude product was purified by flash chromatography and repeated recrystallization.

1,5-bis{4-[3,4-(didodecyloxy)benzoyloxy]phenyl}-3-(thien-2-yl)-6-oxoverdazyl (6a). Crude product was purified by column chromatography (SiO$_2$, CH_2Cl_2/AcOEt 60:1, then SiO$_2$ CH_2Cl_2/petroleum ether 2:1), and recrystallized from diluted AcOEt solution (4x) giving a dark green solid; yield 186 mg (71%); mp 97-98 °C; IR (KBr) 1732 (C=O), 1600, 1506 (C=C), 1276, 1204 (C-O) cm^{-1}; MALDI-MS (*m/z*) 1333.7 (100, [M+Na+H]$^+$), 1282.7 (45, [M-CO]$^+$). Anal. Calcd for $C_{80}H_{117}N_4O_9S$ (1309.9): C, 73.30; H, 9.00; N, 4.27; S, 2.45. Found: C, 73.34; H, 9.01; N, 4.41; S, 2.39.

1,5-bis{4-[3,4,5-(tridodecyloxy)benzoyloxy]phenyl}-3-(thien-2-yl)-6-oxoverdazyl (7a). Crude product was purified by column chromatography (SiO$_2$, CH$_2$Cl$_2$), and recrystallized from CH$_3$CN/CH$_2$Cl$_2$ (9:1) solutions (4x) giving a dark green solid; yield 178 mg (53%); mp 83-84 ^{o}C; IR (KBr) 1731 (C=O), 1697, 1597, 1503 (C=C), 1210, 1120 (C-O) cm^{-1}; MALDI-MS (*m/z*) 1650.5 (100, [M-CO]$^+$). Anal. Calcd for C$_{104}$H$_{165}$N$_4$O$_{11}$S (1679.5): C, 74.37; H, 9.90; N, 3.34; S, 1.91. Found: C, 74.39; H, 9.94; N, 3.41; S, 1.98.

1,5-bis{4-[3,4,5-(tridodecyloxy)benzoyloxy]phenyl}-3-(3-fluorophenyl)-6-oxoverdazyl (7b). Crude product was purified by column chromatography (SiO$_2$, CH$_2$Cl$_2$/petroleum ether 2:1), and recrystallized from CH$_2$Cl$_2$/CH$_3$CN solutions (4x) giving a pink-red solid; yield 208 mg (62%); mp 85-86 ^{o}C; IR (KBr) 1732 (C=O), 1701, 1593, 1503 (C=C), 1339, 1212 (C-O) cm^{-1}; MALDI-MS (*m/z*): 1663.1 (100, [M-CO]$^+$). Anal. Calcd for C$_{106}$H$_{166}$FN$_4$O$_{11}$ (1691.5): C, 75.27; H, 9.89. Found: C, 75.42; H, 9.18.

1,5-bis{4-[3,4,5-(tridodecyloxy)benzoyloxy]phenyl}-3-trifluoromethyl-6-oxoverdazyl (7c). Crude product was purified by column chromatography (SiO$_2$, CH$_2$Cl$_2$/hexane 3:1), and recrystallized from CH$_2$Cl$_2$/CH$_3$CN solutions (4x) giving a wine-red solid; yield 166 mg (50%); mp 57 ^{o}C; IR (KBr) 1737 (C=O), 1589, 1504 (C=C), 1338, 1197 (C-O) cm^{-1}; MALDI-MS (*m/z*): 1637.0 (100, [M-CO]$^+$). Anal. Calcd for C$_{101}$H$_{162}$F$_3$N$_4$O$_{11}$ (1665.2): C, 72.84; H, 9.80. Found: C, 72.82; H, 9.68.

1,5-bis{4-[4-[3,4-(didodecyloxy)benzoyloxy]benzoyloxy]phenyl}-3-(thien-2-yl)-6-oxoverdazyl (8a). Crude product was purified by column chromatography (SiO$_2$, CH$_2$Cl$_2$), and recrystallized from CH$_3$CN/CH$_2$Cl$_2$ (1:1) and then from pentane/CH$_2$Cl$_2$ (3:2) mixtures (4x) giving a dark green solid; yield 173 mg (56%); mp 153 ^{o}C; IR (KBr) 1737 (C=O), 1689, 1600, 1506 (C=C), 1265, 1195, 1160 (C-O) cm^{-1}; MALDI-MS (*m/z*) 1523.1 (100, [M-CO]$^+$). Anal. Calcd for C$_{94}$H$_{125}$N$_4$O$_{13}$S (1551.1): C, 72.79; H, 8.12; N, 3.61; S, 2.07. Found: C, 72.54; H, 8.16; N, 3.61; S, 2.10.

1,5-bis{4-[4-[3,4,5-(tridodecyloxy)benzoyloxy]benzoyloxy]phenyl}-3-(thien-2-yl)-6-oxoverdazyl (9a). Crude product was purified by column chromatography (SiO$_2$, CH$_2$Cl$_2$), and recrystallized from pentane/CH$_2$Cl$_2$ (3:2) followed by CH$_3$CN/CH$_2$Cl$_2$ (10:8) mixtures (4x) giving a dark green solid; yield 196 mg (51%); mp 115 °C; IR (KBr) 1740 (C=O), 1694, 1603, 1505 (C=C), 1265, 1196, 1162 (C-O) cm^{-1}; MALDI-MS (*m/z*) 1891.4 (100, [M-CO]$^+$). Anal. Calcd for C$_{118}$H$_{173}$N$_4$O$_{15}$S (1919.7): C, 73.83; H, 9.08; N, 2.92; S, 1.67. Found: C, 73.83; H, 9.29; N, 2.82; S, 1.67.

1,5-Bis{4-[3-(cholestan-3β-yloxycarbonyl)propionyloxy]phenyl}-3-trifluoromethyl-6-oxoverdazyl (14a). Crude product was purified by column chromatography (SiO$_2$, CH$_2$Cl$_2$) followed by recrystallization from diluted EtOAc/MeCN mixtures (4x) giving an orange solid; yield: 214 mg (83%); mp 196 ^{o}C; [α]$_D^{20}$ = −14.6 (*c* = 0.057, CHCl$_3$); IR (KBr) 1765, 1733 (C=O), 1499 (N-N), 1204, 1170 cm^{-1}; MALDI-MS (*m/z*): 1266.4 (100, [M-CO+H]$^+$). Anal. Calcd for C$_{77}$H$_{110}$F$_3$N$_4$O$_9$ (1292.7): C, 71.54; H, 8.58. Found: C, 71.56; H, 8.50.

1,5-Bis{4-[3-(cholestan-3β-yloxycarbonyl)propionyloxy]phenyl}-3-phenyl-6-oxoverdazyl (14b). Crude product was purified by column chromatography (SiO$_2$, CH$_2$Cl$_2$ gradient CH$_2$Cl$_2$/EtOAc 25:1) followed by recrystallization from CH$_2$Cl$_2$/MeCN (4x) and then from diluted EtOAc solutions (2x) giving a violet solid; yield: 192 mg (74%); mp 219 ^{o}C (decomp.); [α]$_D^{20}$ = −76.7 (*c* = 0.035, CHCl$_3$); IR (KBr) 1761, 1730, 1701 (C=O), 1501 (N-N), 1201, 1166 (C-O) cm^{-1}; MALDI-MS (*m/z*) 1274.0 (100, [M-CO+H]$^+$). Anal. Calcd for C$_{82}$H$_{115}$N$_4$O$_9$ (1300.8): C, 75.71; H, 8.91; N, 4.31. Found: C, 75.68; H, 8.96; N, 4.31.

1-(4-Cyanophenyl)-5-{4-[4-(7,7,8,8,9,9,10,10,11,11,12,12,12-tridecaflurododecyloxy)-benzoyloxy]phenyl}-3-trifluoromethyl-6-oxoverdazyl (20[6,6]). Crude product was purified by column chromatography (SiO$_2$, CH$_2$Cl$_2$) followed by recrystallization from MeCN (4x) giving a dark violet solid: 109 mg (62%); mp 146 °C; IR (KBr) 2222 (C≡N), 1728 (C=O), 1605 (C=C), 1496, 1251, 1208, 1166, 1141 cm^{-1}; MALDI-MS (*m/z*) 854.4 (100, [M-CO]$^+$). Anal. Calcd for C$_{35}$H$_{24}$F$_{16}$N$_5$O$_4$ (882.6): C, 47.63; H, 2.74; N, 7.94. Found: C, 47.56; H, 2.86; N, 7.86.

1-{4-[3-(cholestan-3β-yloxycarbonyl)propionyloxy]phenyl}-5-(4-tolyl)-3-trifluoromethyl-6-oxoverdazyl (21a).
Crude product was purified by column chromatography (SiO$_2$, CH$_2$Cl$_2$) followed by recrystallization from MeCN (4x) giving a claret solid; yield: 154 mg (94%); mp 133 ^{o}C (decomp.); $[\alpha]_D^{20}$ = −41.2 (*c* = 0.036, CHCl$_3$); IR (KBr) 1770, 1726 (C=O), 1502 (N-N), 1201, 1140 (C-O) cm^{-1}; EI-MS (*m/z*) 819.4 (3, [M]$^+$), 371.4 (95, [Cholestane+H]$^+$), 349.1 (100, [M-Cholestane-Succinate+H]$^+$). Anal. Calcd for C$_{47}$H$_{62}$F$_3$N$_4$O$_5$ (820.0): C, 68.84; H, 7.62. Found: C, 68.67; H, 7.65.

1-{4-[3-(cholestan-3β-yloxycarbonyl)propionyloxy]phenyl}-5-(4-cyanophenyl)-3-trifluoromethyl-6-oxoverdazyl (21c). Crude product was purified by column chromatography (SiO$_2$, CH$_2$Cl$_2$) followed by recrystallization from diluted MeCN solutions (3x) giving a red solid; yield: 93 mg (56%); mp 93 ^{o}C; $[\alpha]_D^{20}$ = −15.0 (*c* = 0.049, CHCl$_3$); IR (KBr) 2230 (C≡N), 1768, 1733 (C=O), 1603, 1500 (N-N), 1205, 1144 cm^{-1}; EI-MS (*m/z*) 805.4 (1, [M-CN+H]$^+$), 370.3 (70, [Cholestane]$^+$), 335.1 (100). Anal. Calcd for C$_{47}$H$_{59}$F$_3$N$_5$O$_5$ (831.0): C, 67.93; H, 7.16. Found: C, 68.10; H, 7.43.

Acknowledgements

References and Notes

1. *Stable radicals: fundamentals and applied aspects of odd-electron compounds*; Hicks, R. G., Ed.; John Wiley & Sons: Chichester, 2010.
2. Tamura, R.; Uchida, Y.; Suzuki, K. In *Liquid crystals beyond displays: chemisty, physics, and applications* Li, Q., Ed.; John Wiley & Sons: Hoboken, New Jersey, 2012, p 83-110.
3. Wiley, P. F. in *Chemistry of 1,2,3-Triazines and 1,2,4-Triazines, Tetrazines and Pentazines, The Chemistry of Heterocyclic Compounds*, Willey&Sons, New York 1978, pp 1225-1246.
4. Constantinides, C. P.; Koutentis, P. A. *Adv. Heterocycl. Chem.* **2016**, *119*, 173-207.
   http://dx.doi.org/10.1016/bs.aihch.2016.03.001
5. Neugebauer, F. A. *Tetrahedron* **1970**, *26*, 4853-4857.
   http://dx.doi.org/10.1016/S0040-4020(01)93137-0
6. Gilroy, J. B.; McKinnonm, S. D. J.; Koivisto, B. D.; Hicks, R. G. *Org. Lett.* **2007**, *9*, 4837-4840.
   http://dx.doi.org/10.1021/ol702163a
7. Chemistruck, V.; Chambers, D.; Brook, D. J. R. *J. Org. Chem.* **2009**, *74*, 1850-1857.
   http://dx.doi.org/10.1021/jo8019829
8. Mukai, K.; Shiba, D.; Yoshida, K.; Mukai, K.; Hisatou, H.; Ohara, K.; Hosokoshi, Y.; Azuma, N. *Bull. Chem. Soc. Jpn.* **2005**, *78*, 4114-2123.
   http://dx.doi.org/10.1246/bcsj.78.2114
9. Chahma, M.; Macnamara, K.; A., E.; Alberola, A.; Polo, V.; Pilkington, M. *New. J. Chem.* **2007**, *31*, 1973-1978.
   http://dx.doi.org/10.1039/b706049a
10. Toichi, T.; Teki, Y. *Polyhedron* **2005**, *24*, 2337-2340.
    http://dx.doi.org/10.1016/j.poly.2005.03.116
11. Mihara, N.; Teki, Y. *Inorg. Chim. Acta* **2008**, *361*, 3891-3894.
    http://dx.doi.org/10.1016/j.ica.2008.03.003

12.　Ciofini, I.; Adamo, C.; Teki, Y.; Tuyeras, F.; Laine, P. P. *Chem. Eur. J.* **2008**, *14*, 11385-11405.
　　　http://dx.doi.org/10.1002/chem.200801405

13.　Jasinski, M.; Gerding, J. S; Jankowiak, A.; Gębicki, K.; Romański, J.; Jastrzębska, K.; Sivaramamoorthy, A.;
　　　Mason, K.; Evans, D. H.; Celeda, M.; Kaszyński, P. *J. Org. Chem.* **2013**, *78*, 7445-7454.
　　　http://dx.doi.org/10.1021/jo400843y

14.　Milcent, R.; Barbier, G.; Capelle, S.; Catteau, J.-P. *J. Heterocyc. Chem.* **1994**, *31*, 319-324.
　　　http://dx.doi.org/10.1002/jhet.5570310210

15.　Neugebauer, F. A.; Fischer, H.; Krieger, C. *J. Chem. Soc. Perkin Trans. 2* **1993**, 535–544.
　　　http://dx.doi.org/10.1039/p29930000535

16.　Jankowiak, A.; Pociecha, D.; Monobe, H.; Szczytko, J.; Kaszyński, P. *Chem. Commun.* **2012**, *48*, 7064 -
　　　7066.
　　　http://dx.doi.org/10.1039/c2cc33051b

17.　Davis, E. J.; Goodby, J. W. In *Hadbook of Liquid Crystals*; Goodby, J. W., Collings, P. J., Kato, T., Tschierske,
　　　C., Gleeson, H. F., Raynes, P., Eds.; Wiley-VCH: 2014; Vol. 1, p 27-58.

18.　Demus, D. In *Handbook of Liquid Crystals*; Demus, D., Goodby, J. W., Gray, G. W., Spiess, H.-W., Vill, V.,
　　　Eds.; Wiley-VCH: New York, 1998; Vol. 1, p 133-187.

19.　Goodby, J. W.; Davis, E. J.; Mandle, R. J.; Cowling, S. J. In *Hadbook of Liquid Crystals*; Goodby, J. W.,
　　　Collings, P. J., Kato, T., Tschierske, C., Gleeson, H. F., Raynes, P., Eds.; Wiley-VCH: 2014; Vol. 1, p 231-260.

20.　Chandrasekhar, S. In *Handbook of Liquid Crystals*; Demus, D., Goodby, J., Gray, G. W., Spiess, H.-W., Vill,
　　　V., Eds.; Wiley-VCH: New York, 1998; Vol. 2B, p 749-780.

21.　Jasiński, M.; Szczytko, J.; Pociecha, D.; Monobe, H.; Kaszyński, P. *J. Am. Chem. Soc.* **2016**, *138*, 9421-9424.
　　　http://dx.doi.org/10.1021/jacs.6b06444

22.　Gorecka, E.; Pociecha, D.; Mieczkowski, J.; Matraszek, J.; Guillon, D.; Donnio, B. *J. Am. Chem. Soc.* **2004**,
　　　126, 15946-15947.
　　　http://dx.doi.org/10.1021/ja044597k

23.　Matraszek, J.; Mieczkowski, J.; Pociecha, D.; Gorecka, E.; Donnio, B.; Guillon, D. *Chem. Eur. J.* **2007**, *13*,
　　　3377 – 3385.
　　　http://dx.doi.org/10.1002/chem.200601192

24.　Lehmann, M. In *Top Curr Chem.* ; Tschierske, C., Ed.; Springer-Verlag: Heidelberg, 2012; Vol. 318, p 193-
　　　223.

25.　Reddy, R. A.; Tschierske, C. *J. Mater. Chem.* **2006**, *16*, 907-961.
　　　http://dx.doi.org/10.1039/B504400F

26.　Etxebarria, J.; Ros, M. B. *J. Mater. Chem.* **2008**, *18*, 2919–2926.
　　　http://dx.doi.org/10.1039/b803507e

27.　For example: a) F. C. Yu, L. J. Yu, *Chem. Mater.* **2006**, *18*, 5410–5420;
　　　http://dx.doi.org/10.1021/cm060459d
　　　b) F. C. Yu, L. J. Yu, *Liq. Cryst.* **2008**, *35*, 799–813;
　　　http://dx.doi.org/10.1080/02678290802195697
　　　c) W. Weissflog, U. Dunemann, S. Findeisen-Tandel, M. G. Tamba, H. Kresse, G. Pelzl, S. Diele, U.
　　　Baumeister, A. Eremin, S. Sternb, R. Stannarius, *Soft Matter*, **2009**, *5*, 1840–1847.
　　　http://dx.doi.org/10.1039/b819758j

28.　Yang, A.; Kasahara, T.; Chen, E. K. Y.; Hamer, G. K.; Georges, M. K. *Eur. J. Org. Chem.* **2008**, 4571–4574.
　　　http://dx.doi.org/10.1002/ejoc.200800687

29.　Chen, E. K. Y.; Bancerz, M.; Hamer, G. K.; Georges, M. K. *Eur. J. Org. Chem.* **2010**, 5681–5687.

http://dx.doi.org/10.1002/ejoc.201000789

30. Neugebauer, F. A.; Fischer, H.; Siegel, R.; Krieger, C. *Chem. Ber.* **1983**, *116*, 3461-3481.
    http://dx.doi.org/10.1002/cber.19831161019

31. Matuschek, D.; Eusterwiemann, S.; Stegemann, L.; Doerenkamp, C.; Wibbeling, B.; Daniliuc, C. G.; Doltsinis, N. L.; Strassert, C. A.; Eckert, H.; Studer, A. *Chem. Sci.* **2015**, *6*, 4712-4716.
    http://dx.doi.org/10.1039/C5SC00724K

32. Le, T. N.; Brook, D. J. R. Trevisan T. A. 248th ACS Meeting, San Francisco, CA, Aug 10-14, 2014. Abstract 958-ORGN.

33. Wöhrle, T.; Beardsworth, S. J.; Schilling, C.; Baro, A.; Giesselmann, F.; Laschat, S. *Soft Matter* **2016**, *12*, 3730-3736.
    http://dx.doi.org/10.1039/C5SM02489G

34. Jankowiak, A.; Pociecha, D.; Szczytko, J.; Monobe, H.; Kaszyński, P. *J. Am. Chem. Soc.* **2012**, *134*, 2465-2468.
    http://dx.doi.org/10.1021/ja209467h

35. Jankowiak, A.; Pociecha, D.; Szczytko, J.; Monobe, H.; Kaszyński, P. *Liq. Cryst.* **2014**, *41*, 385-392.
    http://dx.doi.org/10.1080/02678292.2013.828334

36. Jankowiak, A.; Pociecha, D.; Szczytko, J.; Monobe, H.; Kaszyński, P. *J. Mater. Chem. C,* **2014**, *2*, 319-324.
    http://dx.doi.org/10.1039/C3TC31984A

37. Jankowiak, A.; Pociecha, D.; Szczytko, J.; Kaszyński, P. *Liq. Cryst.* **2014**, *41*, 1653–1660.
    http://dx.doi.org/10.1080/02678292.2014.947345

38. Lee, H.; Kim, D.; Lee, H.-K.; Qiu, W.; Oh, N.-K.; Zin, W.-C.; Kim, K. *Tetrahedron Lett.* **2004**, *45*, 1019-1022.
    http://dx.doi.org/10.1016/j.tetlet.2003.11.085

39. Wöhrle, T.; Baro, A.; Laschat, S. *Materials* **2014**, *7*, 4045-4056.
    http://dx.doi.org/10.3390/ma7054045

40. Jasiński, M.; Pociecha, D.; Monobe, H.; Szczytko, J.; Kaszyński, P. *J. Am. Chem. Soc.* **2014**, *136*, 14658–14661.
    http://dx.doi.org/10.1021/ja507594h

41. Ciastek, S.; Jasiński, M.; Kaszyński, P. *RSC Adv.* **2015**, *5*, 33328–33333.
    http://dx.doi.org/10.1039/C5RA04119H

42. Jasiński, M.; Gebicki, K.; Kaszyński, P. *Liq. Cryst.* **2015**, *42*, 982-988.
    http://dx.doi.org/10.1080/02678292.2015.1011718

43. Ciastek, S.; Kaszyński, P.; Pociecha, D.; Jasiński, M. *submitted*.

44. Tschierske, C. *Top. Curr. Chem.* **2012**, *318*, 1-108.
    http://dx.doi.org/10.1007/128_2011_267
    http://dx.doi.org/10.1007/978-3-642-27591-3

45. Gerding, J., M.Sc. Vanderbilt University, 2015.

46. Kapusciński, S., M.Sc. University of Lodz, 2015.

47. Muller-Horsche, E.; Haarer, D.; Scher, H. *Phys. Rev. B* **1987**, *35*, 1273-1280.
    http://dx.doi.org/10.1103/PhysRevB.35.1273

48. Sergeyev, S.; Pisula, W.; Geerts, Y. H. *Chem. Soc. Rev.* **2007**, *36*, 1902–1929.
    http://dx.doi.org/10.1039/b417320c

49. Pisula, W.; Müllen, K. In *Hanbook of Liquid Crystals*; Goodby, J. W.; Collings, P. J.; Kato, T.; Tschierske, C.; Gleeson, H. F.; Raynes, P.; Eds.; Wiley-VCH: Mörlenbach, Germany, 2014; Vol. 8, p 627-673.

50. Suárez, S.; Mamula, O.; Scopelliti, R.; Donnio, B.; Guillon, D.; Terazzi, E.; Piguet, C.; Bünzli, J.-C. G.; *New J. Chem.* **2005**, *29*, 1323–1334;
http://dx.doi.org/10.1039/b503591k
b) Bury, I.; Heinrich, B.; Bourgogne, C.; Guillon, D.; Donnio, B. *Chem. Eur. J.* **2006**, *12*, 8396–8413;
http://dx.doi.org/10.1002/chem.200600449
c) Cristiano, R.; Westphal, E.; Bechtold, I. H.; Bortoluzzi, A. J.; Gallardo, H. *Tetrahedron* **2007**, *63*, 2851–2858;
http://dx.doi.org/10.1016/j.tet.2007.01.045
d) Stone, D. A.; Tayi, A. S.; Goldberger, J. E.; Palmer, L. C.; Stupp, S. I. *Chem. Commun.* **2011**, *47*, 5702–5704;
http://dx.doi.org/10.1039/c1cc10809c
e) Nishikawa, E.; Yamamoto, J.; Yokoyama, H. *Chem. Lett.* **2001**, *30*, 94–95.
http://dx.doi.org/10.1246/cl.2001.94

51. Cholestan-3-yl hydrogen succinate was obtained in two steps and 89% overall yield by diastereoselective hydrogenation of cholesterol using in situ generated Pd(0)/C catalyst (F.-Felpin, X.; Fouquet, E. *Chem. Eur. J.* **2010**, *16*, 12440–12445) followed by reaction of the resulting 3β-cholestanol with excess succinic anhydride, according to the literature procedure: Watabe, J.; Singh, L.; Nakahara, Y.; Ito, Y.; Hojo, H.; Nakahara, Y. *Biosci. Biotechnol. Biochem.* **2002**, *66*, 1904–1914.